Effects of Wind and Effective Emissivity of the Cover on a Passive Solar Still: A Theoretical and Experimental Study

Journal:	*Desalination and Water Treatment*
Manuscript ID:	Draft
Manuscript Type:	Original Paper
Date Submitted by the Author:	n/a
Complete List of Authors:	Jones, J.; Mercer University, Environmental Engineering Lackey, Laura; Mercer University, Environmental Engineering Lindsay, Kevin; Mercer University, Biomedical Engineering
Keywords:	Solar Distillation, Wind effects, Tau effective, Solar Still, Desalination

Title:
Effects of Wind and Effective Emissivity of the Cover on a Passive Solar Still: A Theoretical and Experimental Study

Authors:
J. Andrew Jones
Mercer University School of Engineering
Department of Environmental Engineering
1400 Coleman Ave.
Macon, GA 31207
jonesj12@rpi.edu

Laura W. Lackey (Corresponding Author)
Mercer University School of Engineering
Department of Environmental Engineering
1400 Coleman Ave.
Macon, GA 31207
Office: (478) 301-4106
Fax: (478) 301-2331
lackey_l@mercer.edu

Kevin E. Lindsay
Mercer University School of Engineering
Department of Biomedical Engineering
1400 Coleman Ave.
Macon, GA 31207
kevin.edward.lindsay@live.mercer.edu

Title:

Effects of Wind and Effective Emissivity of the Cover on a Passive Solar Still: A Theoretical and Experimental Study

Abstract:

The development of an accurate thermodynamic model for the basic solar still has been the goal of many researchers. Glass covers are the most common choice of cover material, but are not always available under all situations and pose a large risk of physical injury if not handled with precaution. The effects of using three different cover materials (Glass, Plexiglas, and Plastic Wrap) were investigated under a series of environmental conditions. The heat transfer model has been improved upon by the incorporation of a term for the effective emissivity of the cover, τ_{eff}. The effective τ expands upon the definition of the basic τ by incorporating the reflecting effects of the condensed, but not yet collected water droplets adhered to the interior surface of the cover. The cumulative yield and water temperature profile predictions of the improved model were verified by a comparison to experimental results.

Keywords: Solar Distillation, Tau effective, Solar Still, Desalination, Wind effects

1. Nomenclature and Symbols:

Symbol	Value	Units	Description
t	-	Seconds	Time
α	0.96	-	Absorptivity of the plate
τ_{eff}	Time Variant	-	Effective emissivity of the cover
$Q_{c,p-w}$	Time Variant	W/m^2	Energy transfer from plate to water
Q_{p-o}	Time Variant	W/m^2	Energy transfer from plate to ambient outside air
$Q_{evaporation}$	Time Variant	W/m^2	Energy transfer due to evaporation
$Q_{condensation}$	Time Variant	W/m^2	Energy transfer due to condensation
$Q_{c,g-o}$	Time Variant	W/m^2	Energy transfer from cover to outside ambient air
$h_{c,p-w}$	200	W/m^2 °C	Convective heat transfer coefficient from plate to water
$h_{c,I-o}$	100	W/m^2 °C	Convective heat transfer coefficient from insulation to ambient outside air
$h_{c,g-o}$	200	W/m^2 °C	Convective heat transfer coefficient from cover to outside ambient air
h_{fg}	2.4 x 10^6	J/kg	Latent heat of vaporization for water
C_P	800	J/kg °C	Specific heat capacity of absorption plate
C_w	4184	J/kg °C	Specific heat capacity of seawater
C_A	1006	J/kg °C	Specific Heat Capacity of humid air
C_G	840	J/kg °C	Specific heat capacity of cover material
T_P	Time Variant	°C	Temperature of top of the absorption plate
T_o	Time Variant	°C	Temperature of ambient outside air
T_w	Time Variant	°C	Temperature of top of water
T_A	Time Variant	°C	Temperature of humid air
T_G	Time Variant	°C	Temperature of cover material
M_P	14.4	kg/m^2	Mass density of absorption plate
M_G	8.9(glass), 6.7(Plexiglas), 0.044(plastic wrap)	kg/m^2	Mass density of cover material
V_A	0.028	m^3	Volume of humid air
ρ_w	Time Variant	kg/m^3	Density of seawater
ρ_A	Time Variant	kg/m^3	Density of humid air
L_p	0.010	m	Length/thickness of absorptive plate
L_I	0.038	m	Length/thickness of Styrofoam insulation
b	0.011 (Initially)	m	Thickness of seawater
K_p	0.7	W/m^2 °C	Thermal conductivity of plate
K_I	0.033	W/m^2 °C	Thermal conductivity of insulation
P_{SAT}	Time Variant	Pa	Saturated vapor pressure of water
H_R	Time Variant	-	Relative humidity of vapor inside the solar distillation unit
$m_{condensation}$	Time Variant	kg/m^2	Mass of condensation

2. Introduction and Background:

Ninety-seven percent of the world's available water supply is unfit for human consumption due to its large salt concentration [1]. Multitudes of people around the world suffer from severe water shortages and available potable water sources are becoming a desirable commodity. A procedure known as desalination, removing salts from water, has gained much attention in the literature as a solution to the problem. Large-scale desalination systems are used in many countries around the world, most notably in India and the Middle East where the arid climate causes the production of freshwater to be a necessity [1]. A compact, lightweight solar distillation unit would be beneficial in the immediate aftermath of a natural disaster to provide short-term relief.

The literature is flooded with different designs and configurations for solar distillation (SD) apparatus', many of which contain mathematical models and simulations predicting maximum efficiency. Several excellent reviews have been recently published [2–6]. Reviews specific to active [7] and passive solar distillation [8] are also available. Many investigators have summarized and modeled results for specific locations [9]. All types of SD units exhibit similar problems such as low yields and large surface area to yield ratios.

The components of a single-slope, basin-type SD units are shown in Figure 1 and consist of: An absorptive plate or black surface (1), Water Layer (2), Insulation (3), Humid Air (4), Glass Cover (5), and Collection Trough (6).

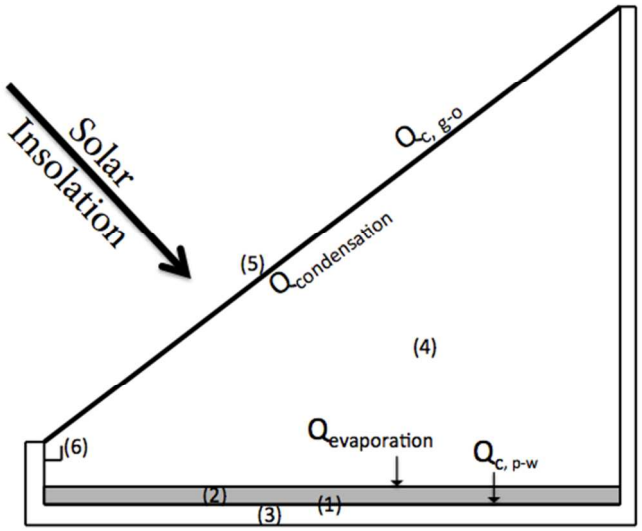

Figure 1. The basic solar still design with labeled components and energy transfers. (1) Absorptive Plate, (2) Seawater, (3) Insulation, (4) Humid Air, (5) Glass Cover, (6) Collection Trough.

A single-slope solar still as shown in Figure 1 is comprised of an insulated box with the top cover made from a material with high transmittance and thermal conductance (most commonly glass). There are three main areas of a simple solar still including: the insulated sides, the absorptive basin to hold seawater, and the cover. The sides of the container are insulated to decrease heat loss from the brine solution through the sides of the apparatus. The basin serves two functions: to hold the seawater and to absorb light energy passing through the seawater before it is lost to the environment. To maximize absorption, the sides and bottom of the container are commonly black. The cover is also multipurpose – it seals the system

from any mass transport to the system surroundings, while still allowing energy in the form of direct thermal insolation to enter. It also serves as the condensation surface to collect the freshwater output. The collection of thermal radiation inside the device will cause the interior temperature to increase causing an increase in the vapor pressure of water in the solution. When the hot water vapor hits the relatively cool cover, the water vapor will condense, form droplets, and with help from gravity, rolls down the inclined plane to be collected in a bottle or trough. Refer to area (6) of Figure 1 for a visual representation of the condensate collection trough.

The goal of this project was to design, build, test, and mathematically model a single-slope SD unit fitted with three unique cover materials including plastic wrap that would typically be found in a kitchen cabinet, glass, and Plexiglas. The effects of the different covers on the temperature and the yield of the system were analyzed and explained with the heat transfer model.

3. Heat Transfer Modeling Equations:

Energy Balances are preformed on primary still components including the absorptive plate, the water in the absorptive basin, the humid air, and for the transparent cover. A differential energy balance around the absorptive plate, as shown in Equation (1), was used to determine the temperature of the plate (T_p). It was assumed that the absorptive plate absorbed all solar insolation and the heat transfer due to radiation was insignificant when compared to that of convection.

$$\Delta E = M_p C_p \frac{dT_p}{dt} = \text{Solar Radiation} - Q_{c,p\text{-}w} - Q_{p\text{-}o} \quad (1)$$

The solar insolation was calculated as

$$\text{Solar Radiation} = I\alpha\tau \quad (2)$$

Equation 3 shows Newton's Law of Cooling that describes the heat transfer by convection from the plate to the water. The thermal resistance model as shown in Equation 4 describes the transfer of energy from the plate to the environment.

$$Q_{c,p-w} = h_{c,p-w}\left(T_p - T_w\right) \quad (3)$$

$$Q_{p-o} = \frac{\left(T_p - T_w\right)}{\frac{L_p}{K_p} + \frac{L_I}{K_I} + \frac{1}{h_{c,I-o}}} \quad (4)$$

Substitution of Equations 2 – 4 into the energy balance for the adsorptive plate yields

$$M_p C_p \frac{dT_p}{dt} = I\alpha\tau - h_{c,p-w}\left(T_p - T_w\right) - \frac{\left(T_p - T_w\right)}{\frac{L_p}{K_p} + \frac{L_I}{K_I} + \frac{1}{h_{c,I-o}}} \quad (5)$$

Two modes of energy transfer were considered to determine T_w. It was assumed that the only heat introduced to the water was from convective heat transfer from the absorptive plate, as shown in Equation 3, and energy was lost due to evaporation ($Q_{evaporation}$).

$$\Delta E = \rho_w C_w b \frac{dT_w}{dt} = Q_{c,p-w} - Q_{evaporation} \quad (6)$$

The energy lost due to evaporation was estimated using the semi-empirical term called the Ryan Correlation [10]. The correlation, from Ryan (1974) is based on

measurements in open water bodies (e.g. lakes and ponds) and implements a velocity term to represent the wind speed in m/s across the fluid surface [10]. Neglecting the wind term in the Ryan Correlation, results in Equation 7 for estimating heat loss from evaporation in the SD unit.

$$Q_{evaporation} = 0.027\left(T_w - T_A\right)^{1/3} P_{SAT}\left(1 - H_R\right) \quad (7)$$

Substituting Equations 3 and 7 into Equation 6 provides the expression used to determine the differential temperature of the water.

$$\rho_w C_w b \frac{dT_w}{dt} = h_{c,p-w}\left(T_p - T_w\right) - 0.027\left(T_w - T_A\right)^{1/3} P_{SAT}\left(1 - H_R\right) \quad (8)$$

The energy transfer for the humid air domain is shown as equation 9.

$$\Delta E_{humid\ air} = \rho_A C_A V_A \frac{dT_A}{dt} = Q_{evaporation} - Q_{condensation} \quad (9)$$

The evaporative heat flux into the air was again modeled using the Ryan Correlation as shown in Equation 7. The heat flux from the air domain is due to the condensation of water and is represented by another semi-empirical formula (Equation 10)[11].

$$Q_{condensation} = 85.0\left(T_A - T_G\right) H_R \quad (10)$$

Substituting Equations 7 and 10 into Equation 9 results in the governing equation used to model heat transfer in the humid air domain.

$$\rho_A C_A V_A \frac{dT_A}{dt} = 0.027\left(T_w - T_A\right)^{1/3} P_{SAT}\left(1 - H_R\right) - 85.0\left(T_A - T_G\right) H_R \quad (11)$$

The energy balance for the cover is presented as Equation 12.

$$\Delta E = M_G C_G \frac{dT_G}{dt} = Q_{condensation} - Q_{c,g-o} \quad (12)$$

Substituting into Equation 12, results in Equation 13 representing the energy balance for the cover domain.

$$M_G C_G \frac{dT_G}{dt} = 85.0\left(T_A - T_G\right)H_R - h_{c,g-o}\left(T_G - T_o\right) \quad (13)$$

4. Modeling Mass Transfer:

The still is assumed to be a closed system, so no mass is transferred into or out of the SD unit boundary. The phase change at the water surface results in an evaporative mass flux that increases the partial pressure of water in the air-vapor mixture. To predict yield, the condensation flux occurring at the air-vapor mixture and cover boundary was considered. A straightforward relationship [11] as shown in Equation 14 links the condensation heat transfer and mass condensation rate.

$$\frac{dm_{condensation}}{dt} = \frac{Q_{condensation}}{\text{Latent Heat of Vaporization}} = \frac{85.0\left(T_A - T_G\right)H_R}{h_{fg}} \quad (14)$$

The rate of condensation is determined having units of kg/s·m^2. Integration over the duration of the SD unit operation results in the total mass of condensate produced per unit area of the still cover (kg/m^2). It is assumed that all condensate is collected with 100% efficiency and none is returned to the water basin.

5. Experimental Setup:

Three solar stills were constructed from locally available Styrofoam coolers; the wall thickness of the coolers was 4 cm. The dimensions of the completed solar stills were: Height – 40 cm, Length – 83cm, and Width – 40cm. The most effective cover angle has been well researched and has lead to conflicting results. A recent excellent review [12] was published on this conflict. The cover angle of 45° was chosen to maximize cover surface area while minimizing the effect of water

droplets dripping back into the basin [13]. The interior of the stills were painted flat black and a 10-cm layer of black aquarium rock (average diameter – 6 mm) was placed in the basin to act as the absorptive plate. The water collection trough consisted of a modified one-half inch CPVC pipe, cut in half lengthwise, and secured to the SD unit housing with clear silicone adhesive. The collection trough was connected to the external collection bottle with commonly available CPVC and PVC fittings. The covers were applied to the angled surface of the solar still using clear silicone adhesive. Three cover materials were evaluated in this study: Glass (thickness = 2.4mm), Plexiglas (thickness = 3mm), and Clear Polyethylene Plastic Wrap (thickness = 0.05mm).

At the onset of each experimental run, the solar stills were loaded with 2-liters of tap water through an access plug cut in the back wall of the cooler. This access plug was then sealed with silicone to reduce leaks to the surroundings.

The temperature of water in the basin was measured using a LM35 Precision centigrade temperature sensor. The sensor supplied a linear temperature response at a slope of 10mV/°C with an accuracy of ±0.5°C. The exposed wires and the LM35 package were coated with silicone for waterproofing. The connecting wires for the temperature sensor were run though the rear access plug and placed directly in the water layer. Solar insulation was measured using a Fisher Scientific Traceable Handheld Digital Light Meter with analog output. Insulation was measured on the

same angle and plane as the solar still covers. The light meter has a specified accuracy of ±5% over the range measured.

The temperature and solar insulation data were recorded using the NI USB-6008 analog to digital converter and LabVIEW software. The entire SD system was manually rotated approximately every hour during testing to follow the sun. Effluent yields were manually measured.

6. Results and Discussion:

The mass and heat transfer equations were solved using Berkeley Madonna, an ordinary differential equations software package designed at the University of California at Berkeley. Material properties, heat transfer coefficients, and system dimensions were coded into Berkeley Madonna. Empirical relationships were used to represent properties that change with system temperatures (water vapor pressure, water density, and air density) or that were specific to the testing day (i.e. ambient temperature and solar intensity). The depth of water in the basin, b, decreased with run time and was modeled as a function of water condensed and collected.

An effective emissivity of the covers, τ_{eff}, was measured using the solar meter to record solar readings from the exterior and interior of the solar still. The fraction of light passing through the cover was taken to be the τ_{eff}. The τ_{eff} represents the emissivity of the respective cover materials as well as the fraction of sunlight reflected by the water droplets condensed on the cover that have not yet been

collected. The τ_{eff} values were observed to vary throughout the day, quickly decreasing a couple hours after sunrise, leveling out during the middle of the day, and rising back to their original level after sunset. The extent of the rise and fall for τ_{eff} varied for the three different cover materials and the τ_{eff} profiles are shown in Figure 2.

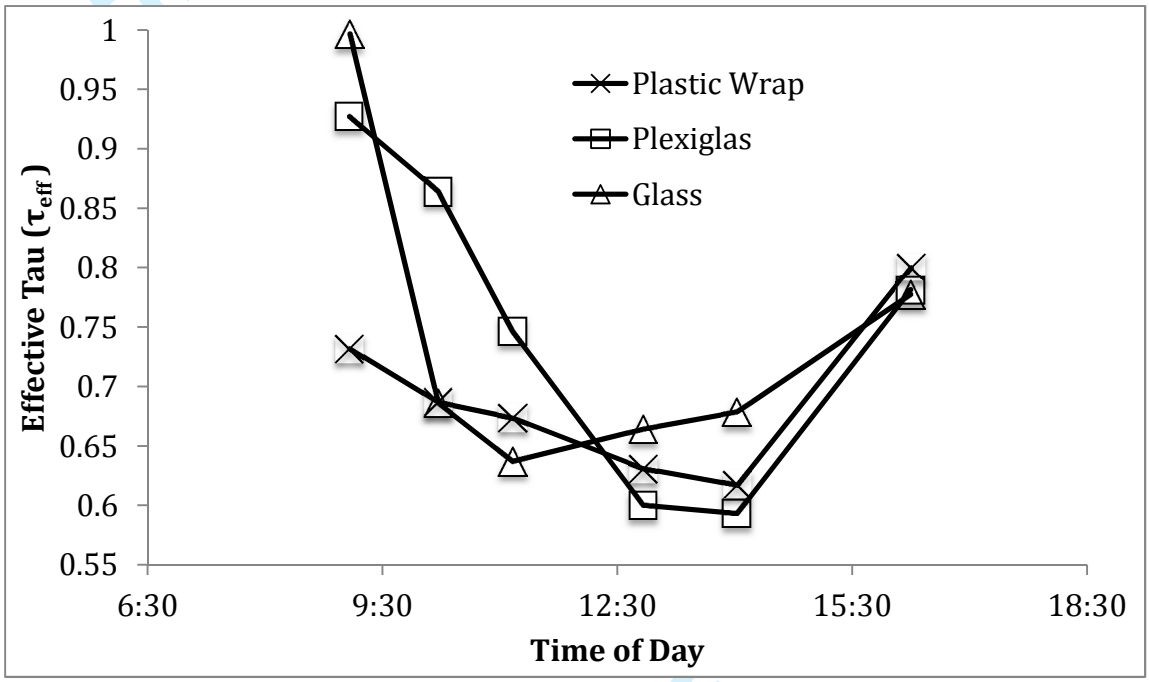

Figure 2. The change of τ_{eff} over the course of the testing day

The measured τ_{eff} profiles were integrated into the model to account for the subsequent decrease in effective insolation available to heat the system.

Water temperature and yield were measured for three different cover materials (Glass (G), Plexiglas (PG), Clear Polyethylene Plastic Wrap (PW)). The data was collected on sunny, clear, precipitation free days; the solar intensity peaked

between 1000 and 1200 W/m^2 on each day and followed a smooth non-skewed parabolic path. The winds were calm through the early part of the day, but picked up toward the early evening. The water temperature profiles were similar in shape for all three solar stills but the maximum temperature was generally higher for G than PG (approx. 2°C) and for PG than PW (approx. 8°C). The output yield of the three systems was highest for the G cover followed by the PW and then the PG.

During a typical testing day the solar stills displayed quick heating during the morning reaching their equilibrium temperature around midday. The rate of freshwater production from the stills was very slow during the morning hours but picked up quickly during the hours of maximum solar insolation immediately preceding midday. Figure 3 displays the solar insolation profile (left axis) and the cumulative yield (right axis) vs. time of day. The sunrise can be observed at 7:30 and the sunset at 19:10 from the solar insolation values. Notice that freshwater production in the morning hours and after sunset are small compared to midday production rates. Production between 12:00 and 16:00 accounted for approximately seventy percent of the cumulative yield.

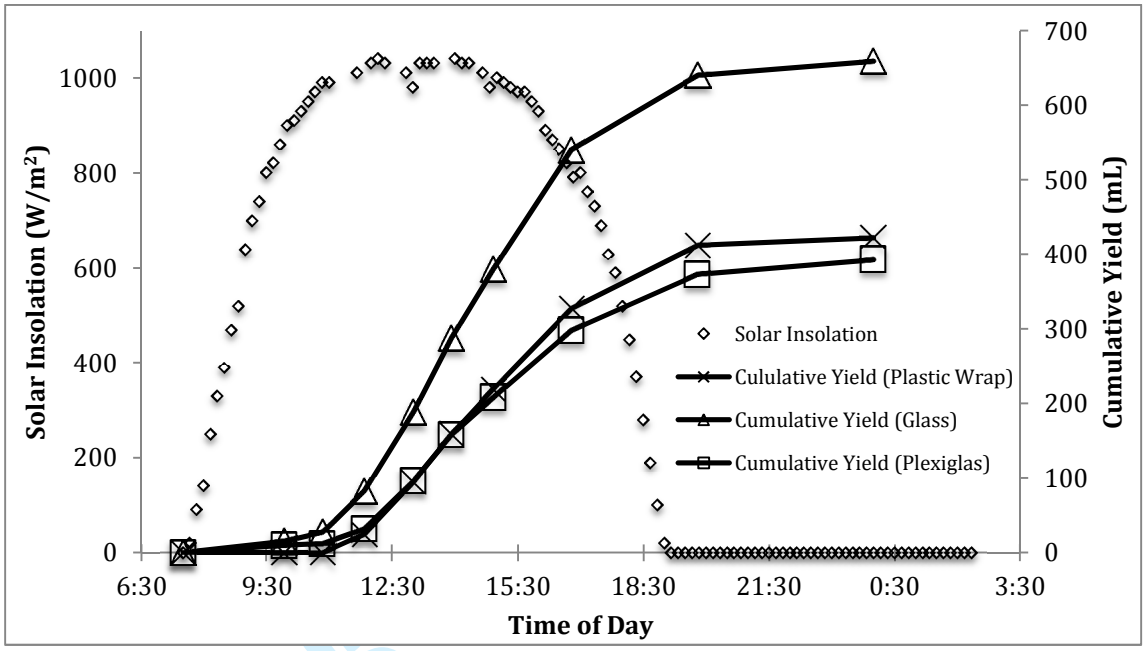

Figure 3. Typical daily relationship between solar insolation and cumulative yield for all three cover materials.

A similar trend was also seen between the typical water temperature and cumulative freshwater yield. Figure 4 shows the similar correlation that approximately seventy percent of the total yield was obtained when the temperature of the water was above 60°C which also corresponds to the time of day from noon to 4pm.

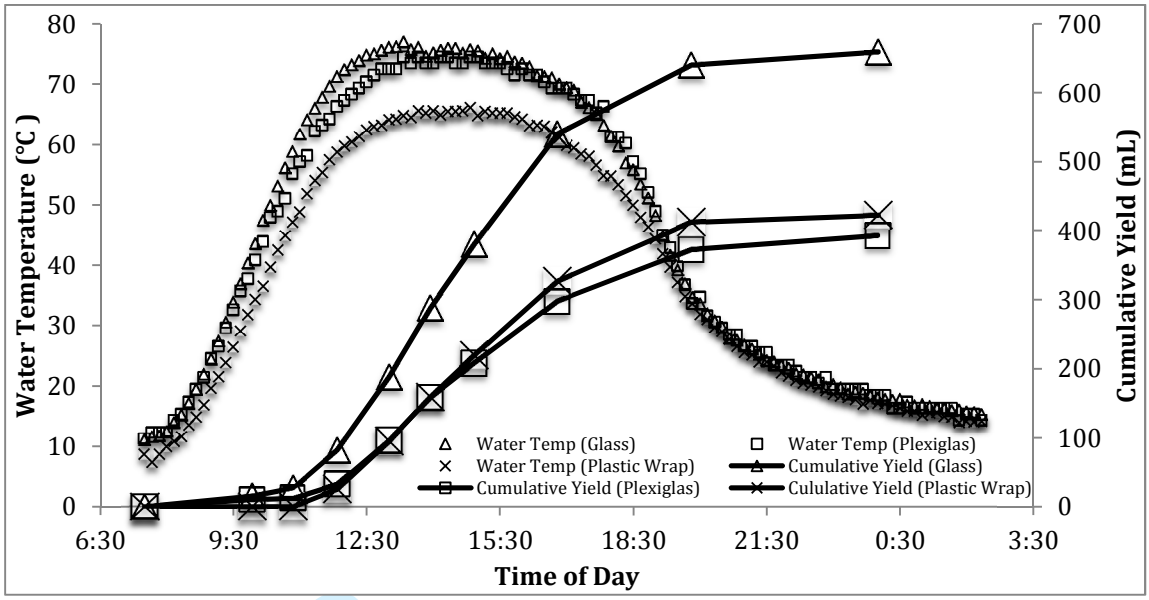

Figure 4. Typical water temperature, ambient air temperature, and cumulative yield vs. time for all cover materials.

The trends shown in Figures 3 and 4 are commonly observed [14–16]. Table 1 summarizes measured data for all cover materials and climatic conditions for multiple days of data collection. The day of October 5th 2011 was used in the comparisons to the thermodynamic model. Thermal and exergy efficiencies were also calculated for the three solar stills as presented by Tiwari et al. [17] and are presented in Table 2.

Table 1. Summary of measured data and climatic conditions for all testing days.

*Data obtained from almanac archives.

Date	Cover Material	Max Water Temperature (°C)	Yield (mL)	Max Solar Insolation (W/m^2)	Ave. Wind Speed (m/s)*	Max/Min Ambient Temperature (°C)*	Weather*
10/5/11	Glass	76.9	659				
	Plexiglas	74.4	393	1040	0.72	29 / 6	Sunny
	Plastic Wrap	66.1	422				
10/6/11	Glass	69.3	621				
	Plexiglas	68.3	390	1050	1.23	29 / 9	Sunny
	Plastic Wrap	61.0	424				
3/17/11	Glass	75.8	668				
	Plexiglas	67.7	367.5	1240	1.23	25 / 2	Sunny
	Plastic Wrap	65.8	340				
3/18/11	Plexiglas	64.9	489	1250	0.21	29 / 3	Partially
	Plastic Wrap	68.3	325				Cloudy
3/23/11	Glass	64.0	293				
	Plexiglas	62.1	245	1377	2.00	29 / 11	Cloudy
	Plastic Wrap	57.4	142				

Table 2. Thermal energy and exergy efficiencies for three solar still cover types.

Cover Material	Thermal Efficiency (%)	Exergy Efficiency (%)
Glass	25.1 ± 2.3	3.6 ± 0.3
Plexiglas	14.9 ± 2.2	3.4 ± 0.4
Plastic Wrap	15.5 ± 3.4	3.0 ± 0.2

The effects of wind (sustained and gusts) on the solar still were not incorporated into the thermodynamic model. Wind affects the solar still by increasing the heat transfer from the cover to the outside ambient air due to forced convection [18] and by forcing micro movement of the cover giving the condensed, but not yet collected, water droplets sufficient energy to overcome contact angle hysteresis [19] and slide down the cover to the collection trough. At low sustained speeds, the wind was shown to increase the output of the solar still up to a point where a further increase in wind speed was then detrimental to the yield due to excessive

movement of the cover such that droplets adhered to the cover surface were disturbed and fell from the cover back to the water reservoir without being collected. This correlation is shown in Figure 5 below. The data was fitted with a second order polynomial to represent the phenomena described above. The days represented in Figure 5 were selected to minimize the effects of other (non-wind) parameters on yield. The small differences in climatic conditions for the testing days are described in Table 1.

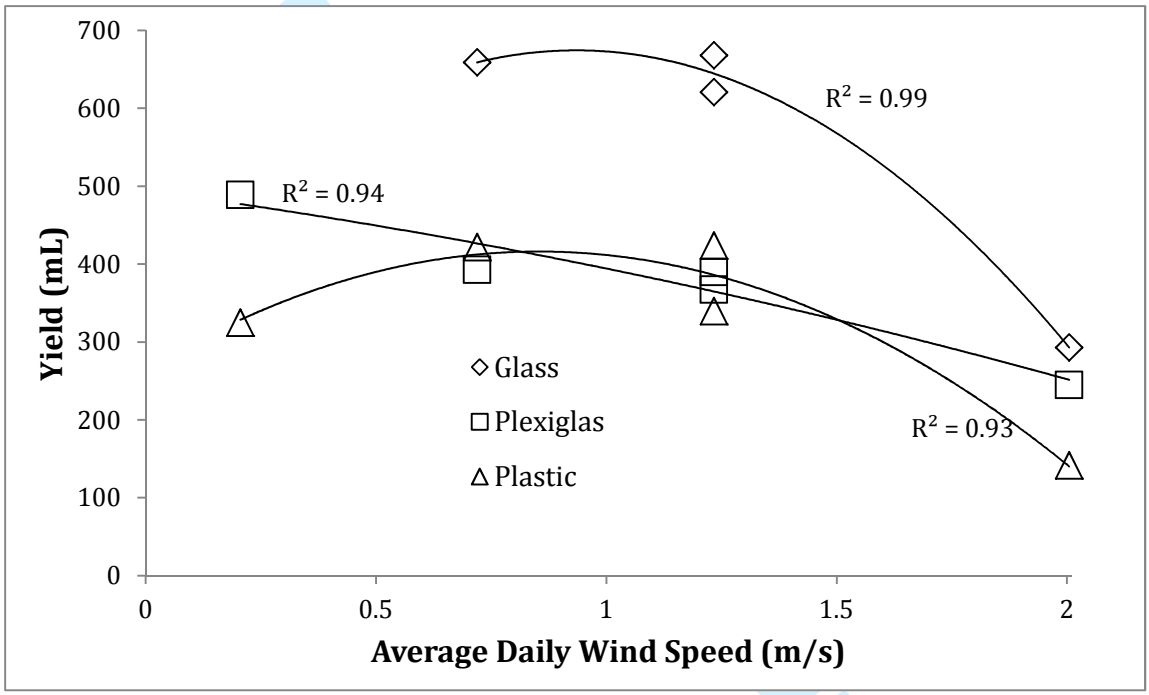

Figure 5. Relationship between the average daily wind speed and the yield of a solar distillation device. Second-order lines of best fit are shown with associated R^2 values.

The effect of wind speed on solar distillation production is controversial. A variety of researchers have shown that an increase in wind speed increases production [14], [20–23], while others have shown increased wind speeds to cause a decrease

in productivity [24–27]. Recent theoretical modeling performed by El-Sebaii indicate that in single incline passive solar still there is a critical mass (or depth) of basin water beyond which the productivity increases with the increase of wind speed, up to some critical wind speed. For SD basins containing less than the critical mass of water, an increase in wind speed causes a decrease in productivity. If the critical wind speed is realized or exceeded, it is predicted to have minimal influence on production [28], [29]. As described by El-Sebaii (2004) the critical mass density of basin water was shown to be 45 kg H_2O/m^2 of plate surface area. The relative initial condition for our work was 11 kg H_2O/m^2 of plate surface area. We observed an increase in production when wind speeds were generally less than 1 m/s, suggesting that system variables other than critical depth influence wind speed impact on production.

Comparing the modeling results to the experimental data showed the efficacy of the thermodynamic model. Experimental data was taken regarding yield and internal water temperature of solar stills with the three different cover materials. Figure 6 presents the cumulative freshwater yields versus time where the lines indicate modeling predictions and the markers indicate experimental data points. A statistical analysis of the data indicates the modeling results fit (R^2>0.9, NRMS error < 5.6%) the experimental temperature and yield profiles. The R^2 values and normalized RMS error calculations for the aforementioned correlations have been presented on the appropriate figures below.

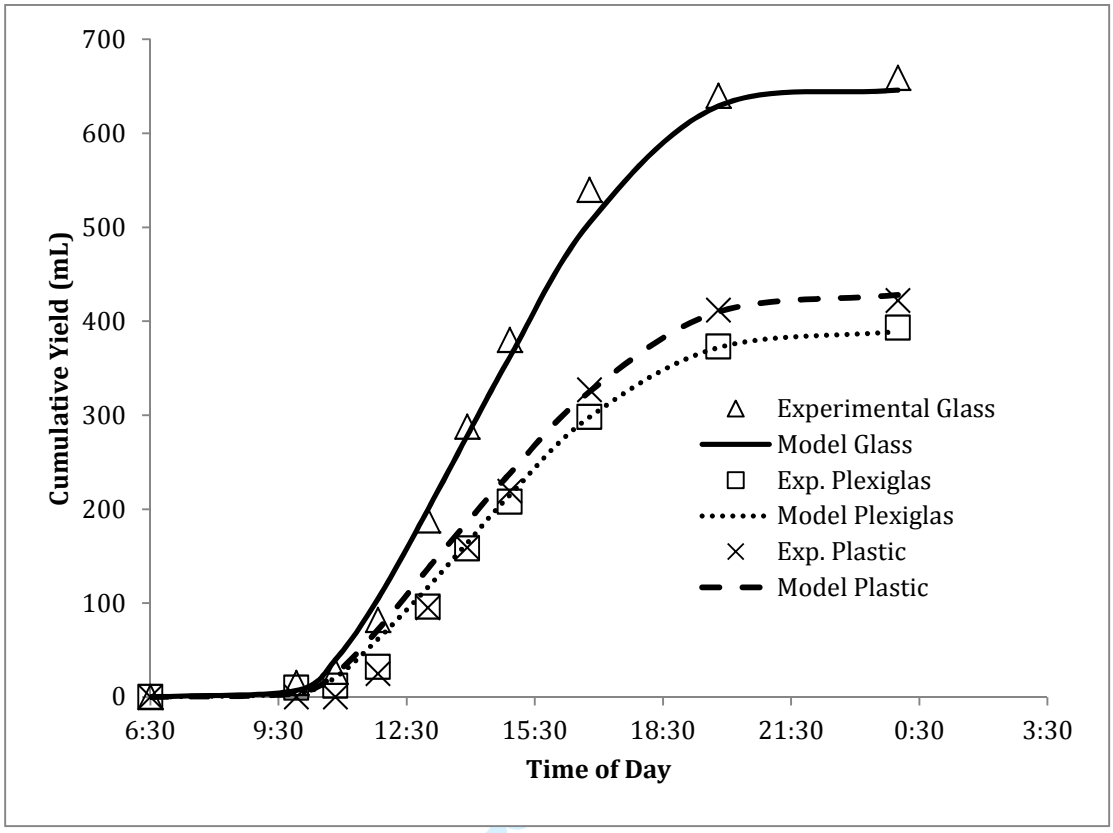

Figure 6. Efficacy of the model for predicting freshwater yield. A comparison was done to the experimental data collected for three cover types on October 5th. Normalized RMS error for glass, Plexiglas, and plastic wrap was found to be 2.6%, 3.2%, and 5.6%, respectively.

Temperature data from the same day was also compared to the modeling results. The results seen in Figures 7-9 show a good fit for the data through the morning and afternoon.

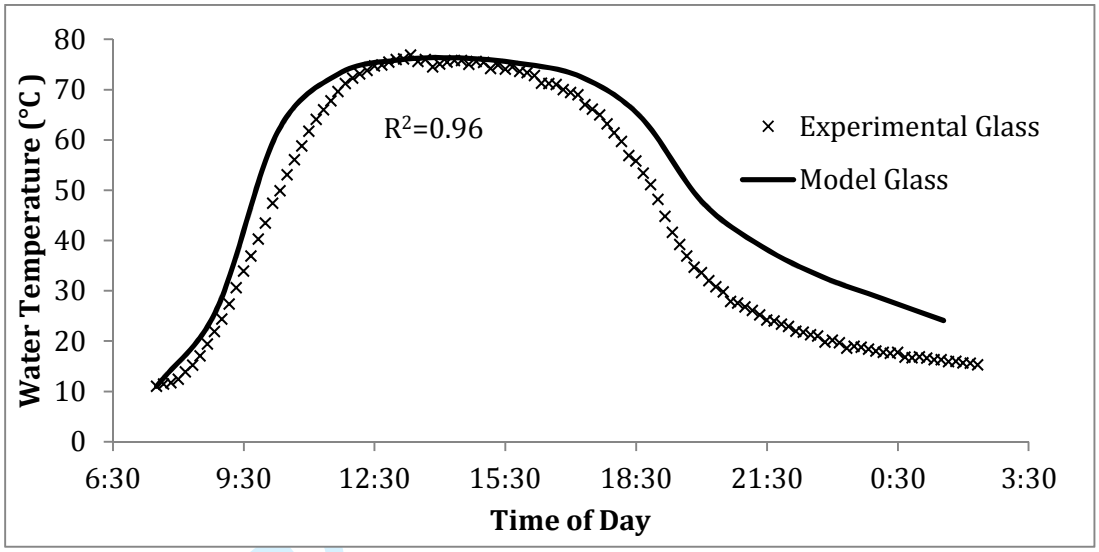

Figure 7. Modeling and experimental comparison of water temperature profiles for a solar still with a glass cover. Normalized RMS error calculated to be 13.2%.

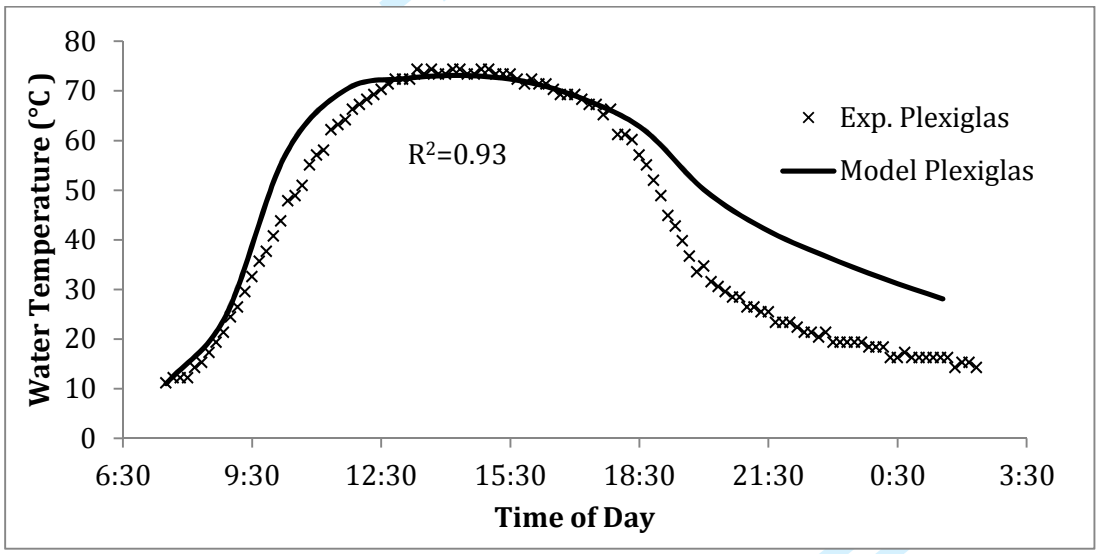

Figure 8. Modeling and experimental comparison of water temperature profiles for a solar still with a Plexiglas cover. Normalized RMS error calculated to be 15.3%.

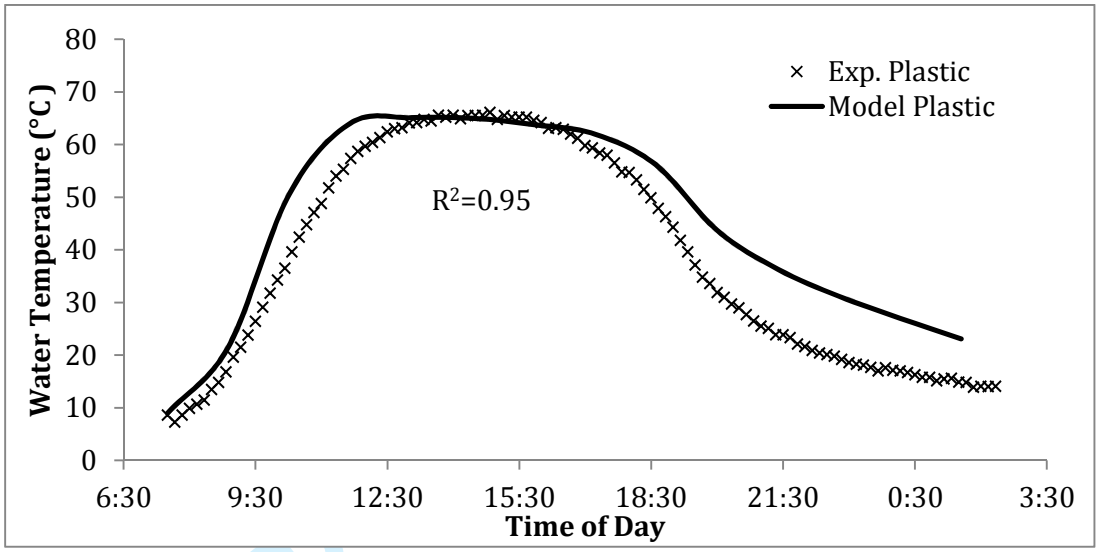

Figure 9. Modeling and experimental comparison of water temperature profiles for a solar still with a plastic wrap cover Normalized RMS error calculated to be 13.9%.

After sunset the theoretically-predicted temperature profiles digress from the observed experimental temperatures, decreasing at a much greater rate than predicted by the model. Forced convection across the cover due to windy afternoon conditions provides a plausible explanation for the observed increase in cooling rate. Almanac data from the testing date indicates that the wind speeds were elevated from 14:00 until 18:00. Figure 10 shows the graph of wind speed almanac data for October 5th.

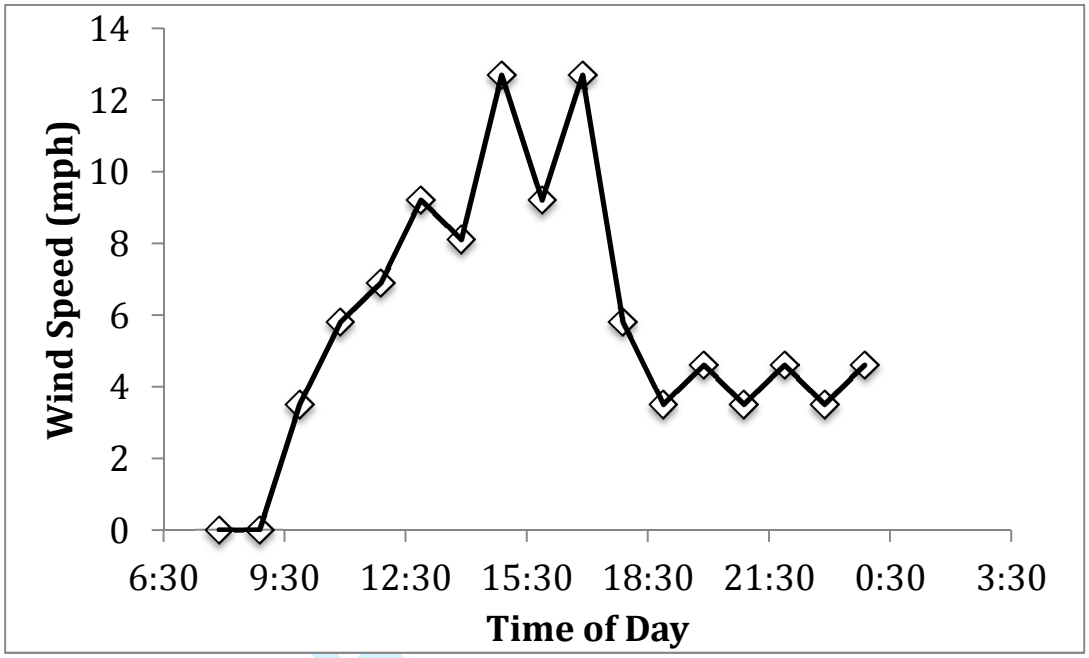

Figure 10. Wind speed profile for October 5th.

The substantial difference between experimental and model-predicted evening temperatures, due to the windy conditions, did not affect the yield predictions or observations. We conclude that this is from the timing of the elevated sustained winds. The highest sustained winds appeared beginning at 15:00 and continuing until 18:00. The hours of highest yield production occurred from 12:00 until 16:00. The small time overlap between these regions was not enough to cause a substantial change in the experimental freshwater production; therefore, resulting in theoretical and experimental yield profiles displaying higher coefficients of determination, R^2, than as compared to the corresponding temperature profiles.

7. Conclusion:

Single slope solar distillation units equipped with three different cover materials were designed, built, and tested. Cover materials used included glass, Plexiglas,

and plastic wrap. The highest internal water temperature and freshwater yield was consistently produced by the solar still fitted with a glass cover. The Plexiglas cover resulted in higher (8°C) water temperature but slightly lower (7%) freshwater yield than the solar still equipped with a plastic wrap cover. A convective heat transfer thermodynamic model for a basic solar still was developed. Good agreement between simulation and experimental results (R^2>0.93) were observed. Improvements can be made to the model by taking into account the effects of wind. These effects include: forced convection from the cover to the ambient air and the addition of kinetic energy to the water collection process. The development of a parameter for the effective emissivity of the cover, τ_{eff}, allows the model to account for the decrease in incoming solar insulation due to the reflection of sunlight by the condensed, but not yet collected, water droplets adhered to the internal surface of the cover. The general trend and expected results are all consistent between the model and experimental data indicating the validity of the differential model.

8. Works Cited:

[1] A. D. Khawaji, I. K. Kutubkhanah, and J. Wie, "Advances in seawater desalination technologies," *Desalination*, vol. 221, pp. 47-69, 2008.

[2] E. Mathioulakis, V. Belessiotis, and E. Delyannis, "Desalination by using alternative energy: Review and state-of-the-art," *Desalination*, vol. 203, pp. 346-365, 2007.

[3] S. Kalogirou, "Seawater desalination using renewable energy sources," *Progress in Energy and Combustion Science*, vol. 31, no. 3, pp. 242-281, 2005.

[4] A. Kaushal, "Solar stills: A review," *Renewable and Sustainable Energy Reviews*, vol. 14, no. 1, pp. 446-453, Jan. 2010.

[5] G. N. Tiwari, H. P. Garg, and H. Khas, "Studies on various designs of solar distillation systems," *Technology*, vol. 1, no. 3, pp. 161-165, 1985.

[6] G. N. Tiwari, H. N. Singh, and R. Tripathi, "Present status of solar distillation," *Solar Energy*, July, 2003.

[7] K. Sampathkumar, T. V. Arjunan, P. Pitchandi, and P. Senthilkumar, "Active solar distillation—A detailed review," *Renewable and Sustainable Energy Reviews*, vol. 14, no. 6, pp. 1503-1526, Aug. 2010.

[8] R. Balan, J. Chandrasekaran, S. Shanmugan, B. Janarthanan, and S. Kumar, "Review on passive solar distillation," *Desalination*, vol. 28, pp. 217-238, 2011.

[9] H. N. Singh and G. N. Tiwari, "Monthly performance of passive and active solar stills for different Indian climatic conditions," *Energy*, vol. 168, pp. 145-150, 2004.

[10] T. P. Yilmaz and H. S. Aybar, "Evaluation of the correlations for predicting evaporative loss from water body," in *ASHRAE Transactions*, 1999, p. 185.

[11] H. Ş. Aybar, "Mathematical modeling of an inclined solar water distillation system," *Desalination*, vol. 190, pp. 63-70, Apr. 2006.

[12] A. J. N. Khalifa, "On the effect of cover tilt angle of the simple solar still on its productivity in different seasons and latitudes," *Energy Conversion and Management*, vol. 52, pp. 431-436, Jan. 2011.

[13] R. Dev and G. N. Tiwari, "Characteristic equation of a passive solar still," *Desalination*, vol. 245, pp. 246-265, 2009.

[14] O. Badran, "Experimental study of the enhancement parameters on a single slope solar still productivity," *Desalination*, vol. 209, no. 1-3, pp. 136-143, Apr. 2007.

[15] M. Afrand, A. Behzadmehr, and A. Karimipour, "A Numerical Simulation of Solar Distillation for Installation in Chabahar-Iran," *Engineering and Technology*, pp. 515-520, 2010.

[16] I. Al-hayek and O. Badran, "The effect of using different designs of solar stills on water distillation," *Mechanical Engineering*, vol. 169, pp. 121-127, 2004.

[17] G. N. Tiwari, V. Dimri, and A. Chel, "Parametric study of an active and passive solar distillation system: energy and exergy analysis," *Desalination*, vol. 242, pp. 1-18, 2009.

[18] P. K. Abdenacer and S. Nafila, "Impact of temperature difference (water-solar collector) on solar-still global efficiency," *Desalination*, vol. 209, pp. 298-305, Apr. 2007.

[19] M. Luo, R. Gupta, and J. Frechette, "Modulating contact angle hysteresis to direct fluid droplets along a homogenous surface," *ACS applied materials & interfaces*, Jan. 2012.

[20] P. I. Cooper, "Digital simulation of transient solar still processes," *Solar Energy*, vol. 12, no. 3, pp. 313-331, 1969.

[21] S. H. Soliman, "Effect on wind on solar distillation," *Solar Energy*, vol. 13, no. 4, pp. 403-415, July 1972.

[22] A. K. Rajvanshi, "Effect of various dyes on solar distillation," *Solar Energy*, vol. 27, no. 1, pp. 51-65, Jan. 1981.

[23] H. P. Garg and H. S. Mann, "Effect of climatic, operational and design parameters on the year-round performance of single-sloped and double-sloped stills under Indian arid zone conditions," *Solar Energy*, vol. 18, no. 2, pp. 15-164, 1976.

[24] K. G. . Hollands, "The regeneration of lithium chloride brine in a solar still for use in solar air conditioning," *Solar Energy*, vol. 7, no. 2, pp. 39-43, 1963.

[25] H. Yeh and L. Chen, "Basin-type solar distillation with air flow through the still," *Energy*, vol. 10, no. 11, pp. 1237-1241, 1985.

[26] H. Yeh and L. Chen, "The effects of climatic, design and operational parameters on performance of wick-type solar distillers," *Energy Conversion and Management*, vol. 26, no. 2, pp. 175-180, 1986.

[27] J. A. Eibling, S. G. Talbert, and G. O. G. Lof, "Solar stills for community use - digest of technology," *Solar Energy*, vol. 13, no. 2, pp. 263-276, 1971.

[28] A. A. El-Sebaii, "Effect of wind speed on active and passive solar stills," *Energy Conversion and Management*, vol. 45, pp. 1187-1204, 2004.

[29] A. A. El-Sebaii, "On effect of wind speed on passive solar still performance based on inner/outer surface temperatures of the glass cover," *Energy*, vol. 36, pp. 4943-4949, 2011.